Bloch oscillations of excitonic wave packets in semiconductor superlattices

P. Leisching, P. Haring Bolivar, W. Beck, Y. Dhaibi, F. Brüggemann, R. Schwedler, and H. Kurz
Institut für Halbleitertechnik II, Rheinisch-Westfälische Technische Hochschule Aachen, D-52056 Aachen, Germany

K. Leo
Institut für Angewandte Photophysik, Technische Universität Dresden, D-01062 Dresden, Germany

K. Köhler
Fraunhofer-Institut für Angewandte Festkörperphysik, D-79108 Freiburg, Germany
(Received 6 May 1994; revised manuscript received 20 July 1994)

We present a detailed investigation of the coherent dynamics of excitonic wave packets composed of heavy/light-hole, electron miniband, and Wannier-Stark states in GaAs/$Al_xGa_{1-x}As$ superlattices. Using transient degenerate four-wave mixing, we study the dependence of Bloch oscillations and heavy/light-hole beats on the applied field, miniband width, lattice temperature, and excitation conditions. Bloch oscillations are observed in samples with minibandwidths varying from 13 to 46 meV and at lattice temperatures up to 200 K. Under certain excitation conditions, we observe higher harmonics of the Bloch oscillation frequency. Spectrally resolved transient four-wave mixing experiments show unambiguously that quantum-mechanical interference is the origin of the oscillations. The experimental four-wave mixing traces are compared with a theoretical model based on many-level third-order density-matrix theory.

I. INTRODUCTION

One of the most fascinating solid state phenomena occurs when an electron can be accelerated by an electric field to a considerable energy relative to the width of the energy band. In the absence of scattering processes and interband tunneling such an electron is Bragg reflected at the Brillouin zone boundary and performs a periodic motion in k and real space, the so-called Bloch oscillation.

In 1928 Bloch[1] started with the investigation of the motion of an electron wave packet with a narrow distribution in $\vec{k}$ space (the quantum-mechanical "Houston states"[2]) in a periodic potential with an external applied electric field $\vec{F}$. The equations of motion for a Bloch electron in $\vec{k}$ space are determined by the acceleration theorem and the energy dispersion relation $E(k)$. In the simplest one-dimensional tight-binding approach, which is sufficient for a homogeneous field F in only one dimension, the energy dispersion $E(k)$ can be approximated by a cosinelike function (see left part of Fig. 1): $E(k) = \Delta/2 = [1 - \cos(kd)]$ with the lattice constant d and the zero field energy bandwidth Δ.

Thus the electron gains energy from the field and moves in k space and also accelerates in real space:[3] the velocity $v(k)$ is illustrated in the left part of Fig. 1. If the electron Bloch wave-packet frequently loses the energy gained from the field by scattering processes (e.g., carrier-carrier, phonon, and interface scattering) it will always stay in an energy region close to the band edge, see Fig. 1 (insets I and II). In the time average, it will thus be transported in the field direction with a constant drift velocity. In the absence of any scattering processes, the electron reaches a k-vector region where the velocity decreases with increasing k (inset III). This leads to the occurrence of negative differential velocity and conductance.[4] If the electron even reaches the upper band edge [i.e., the zone boundary (inset IV)], it reverts its direction undergoing a Bragg reflection, if it does not tunnel into higher energy bands.[5] In this ideal case, the electron will perform a periodic motion in k and also in real space, with the Bloch oscillation time period of

$$\tau_B = \frac{h}{eFd} \tag{1}$$

and an oscillation amplitude in real space

$$L = \frac{\Delta}{2eF}. \tag{2}$$

Equation (1) is even valid for arbitrarily shaped dispersion relations.[6] The coherent carrier motion is restricted to a region of length $2L$. This oscillation time period and the amplitude or localization length are the essential features of Bloch oscillations.

The field-induced Bloch oscillations (BO's) in k space and real space are closely related to the formation of a Wannier-Stark ladder[7] (WSL) in energy space: in the tight-binding approximation the equations of motion can also be solved in energy space. This leads to Wannier-Stark (WS) states Φ^n_{WS} as eigenfunctions, which localize by increasing the field: $\Delta L \simeq \Delta/eF$. Since both the Houston states and the Wannier-Stark states are complete sets of basis functions, we can describe any electronic wave packet with both of them.[8–12] The two pictures are completely inequivalent: the harmonic periodic modulation

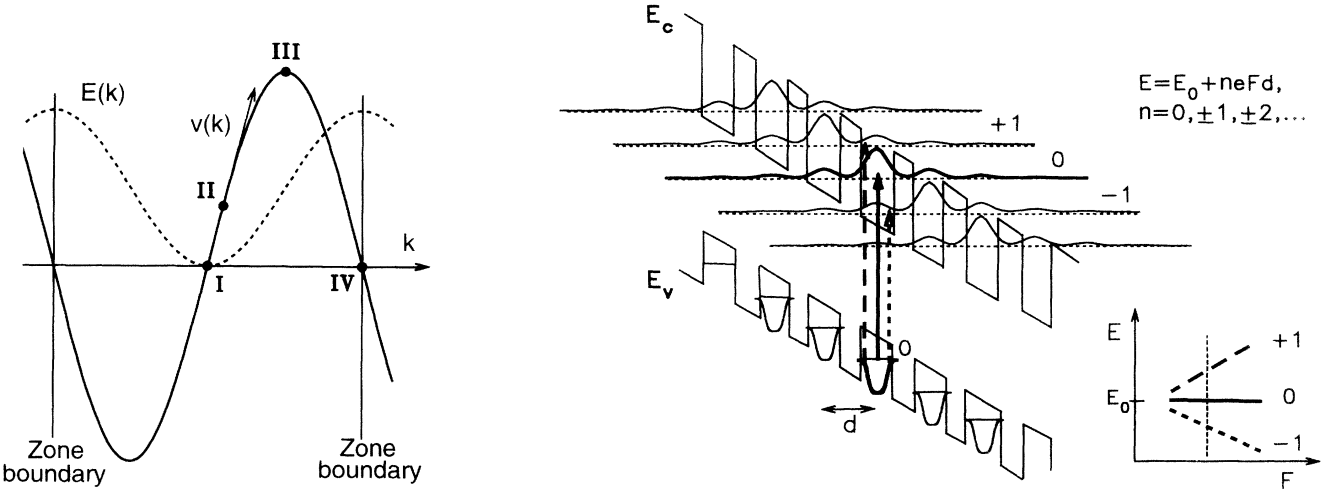

FIG. 1. Left part: Scheme of Bloch oscillations in the Brillouin $z = 1$ (after Ref. 3). The position of the electron in k space is labeled by I–IV. The electron (I) accelerates according to the acceleration theorem. If the k vector reaches the Brillouin zone boundary, it is Bragg reflected and reverts its real space velocity (IV). Right part: Scheme of a WSL in a semiconductor SL. The hh wave function Φ_{WS}^{hh} is already localized even at very low fields due to the large hh mass. The electron wave function Φ_{WS}^{el} is extended over several SL periods at intermediate fields. The WS transitions hh_0 and $hh_{\pm 1}$ are depicted.

with the BO frequency τ_B in the time domain leads to the evolution of Fourier components in the frequency domain with the spacing $\Delta\nu = 1/\tau_B$. Therefore the optical absorption calculated with these eigenstates shows an evenly spaced ladder,[6–8,13] with corresponding eigenenergies

$$E_n = E_0 + n\Delta E, \quad n = 0, \pm 1, \pm 2, \ldots \tag{3}$$

and with the spacing $\Delta E = eFd = h/\tau_B$. The concepts discussed above have been known for many years, but until some time ago there was little hope of ever observing these phenomena in natural solids,[3] due to the large differences in scattering times and BO time by orders of magnitude.

The advent of the man-made semiconductor superlattice (SL), as proposed by Esaki and Tsu,[4] greatly improved the chances for the experimental observation of the WSL and the BO. The main advantage of the SL is the large lattice constant, which leads to (mini)bandwidths much smaller than in a crystal lattice. Typical SL's have periods about a factor of 30 larger than the crystal periods, thus requiring an electric field 30 times smaller to achieve the same BO period. Due to the excitonic effects that are not quenched by the applied field (up to 50 kV/cm) as in the case of bulk materials,[14] the dephasing time is rather long, on the order of a few picoseconds.[15] The electron (el) and heavy-hole (hh) wave functions in a SL for a moderate electric field are depicted in the right part of Fig. 1. At moderate fields, i.e., 10 kV/cm, the electrons are delocalized in contrast to the heavy holes, due to the difference in their masses.

The rapid progress in the growth of high-quality SL has led to an impressive confirmation of the theoretical concepts outlined above. Using continous wave (cw) optical techniques, hh and light-hole (lh) WSL's were observed by many groups.[16–24] Although the miniband is broken into WS levels at even very low fields, we only speak of the WS regime if the separation of the levels is larger than the intrinsic broadening of the levels, i.e., the levels can be resolved.[16] At high applied fields ($L < d$) the wave functions are localized in only one well and the SL has transformed to a multiple-quantum-well system.

In the pioneering experiments performed by Mendez *et al.*[17] and Voisin *et al.*,[18] several transitions of the WSL were clearly resolved. Further experiments demonstrated that the WSL states extend over more than ten wells[19,20] and can even be observed at room temperature.[16] The coexistence of the WSL and negative differential velocity was shown by Sibille *et al.*[21] Theoretical and experimental investigations have shown that the WSL behavior is also observed, albeit with some quantitative changes, when the excitonic correlation of photoexcited electron-hole pairs is considered.[22,23] The transition from Franz-Keldysh oscillations to the WSL in the absorption of a large miniband SL was discussed by Schneider *et al.*[24]

Recent wave-packet experiments in semiconductor SL's have successfully demonstrated the interference of WSL states using transient four-wave mixing.[25–29] The internal electric field associated with the macroscopic Bloch dipole can be measured by a time-resolved electro-optic method.[29,30] In tetrahertz-emission experiments with a SL,[31,32] a widely tunable emission originating from BO's was observed. The discussion of the BO amplitude has recently been addressed in detail in Refs. 33 and 34.

The time-resolved optical experiments performed in a biased semiconductor SL can be easily discussed on the basis of the WS states, i.e., the energy eigenstates. The excitation of an electron-hole wave packet with a first

short laser pulse can then be described by a superposition $\Psi^{el}(z,t)$ and $\Psi^{hole}(z,t)$ of only a few WS states. With a second laser pulse one probes the temporal evolution of the coherent superposition of WS states, which is caused by the different phase factors of the constituents of the packet, leading to interference effects (termed quantum beats). If the Coulomb interaction between electrons and holes is neglected and the hole is assumed to be localized, it is then the electron-hole separation which undergoes the BO. The time dependence of the wave packet is entirely contained in the phase factors $e^{-i\omega_n t}$ of

$$\Psi^{el}(z,t) = \sum_n c_n \exp(-i\omega_n t)\Phi^n_{WS}(z), \quad (4)$$

with ω_n the energy of the transition with index n. The weighting c_n is given by the absorption of the single levels and the spectrum of the exciting laser pulse.

In this paper, we present the results of an extensive study of coherent excitonic wave packets in semiconductor SL's using transient four-wave mixing (FWM). First, we present the experimental setup and the method of preparation of the samples (Sec. II). In the subsequent sections we investigate the dependence of the oscillations on various experimental parameters: (i) applied electric field (Sec. III), where we discuss the dependence of the oscillation period, amplitude, and Zener tunneling on the field, (ii) miniband width (Sec. IV), in which we discuss the observation of BO and hh/lh beats in minibands from 13 meV to 46 meV; (iii) lattice temperatures up to 200 K (Sec. V); and (iv) different excitation conditions of the Bloch wave packet (Sec. VI). We show that coherent control of the wave-packet shape and oscillation frequency is possible and consistent with theoretical calculations. By spectrally resolving the diffracted signal, we prove that the signals observed indeed result from the quantum interference of Wannier-Stark states (Sec. VII). The paper is concluded by a brief summary (Sec. VIII). Appendixes A and B give the theoretical background for the numerical and density-matrix calculations.

II. SAMPLES AND EXPERIMENT

For the investigation, we choose GaAs/$Al_xGa_{1-x}As$ SL's due to their superior quality and optical transitions in an easily accessible wavelength range. The samples are grown by molecular beam epitaxy on n-doped GaAs substrate with a 2500 Å undoped $Al_xGa_{1-x}As$ buffer beneath the SL region and a 3500 Å undoped $Al_xGa_{1-x}As$ buffer at the top. The undoped SL structure contains 35 periods of wells and barriers, with constant barrier thickness (17 Å) and aluminum content ($x = 0.3$). We use five different well widths: 61, 67, 80, 97, and 111 Å. The samples are labeled according to their period length d: sample 78, 84, 97, 114, and 128 Å. From sample 114 Å we study two samples from two different wafers with different optical and electrical qualities. To apply electric fields, we evaporate an Ohmic contact on the n-doped substrate and a transparent Cr/Au Schottky contact on the front side. Part of the substrate is removed by selective wet etching to allow experiments in transmission configuration.

The widths of the electrons and the hh/lh lowest miniband are derived from a Kronig-Penney calculation. The results are listed in Table I.

The width of the lh miniband is comparable to that of the electrons. Therefore the lh will also remain delocalized in an el/lh wave packet and will produce a more complex dynamic than an el/hh wave packet where the hh is strongly localized.

The samples are carefully characterized using cw photoluminescence (PL) and photocurrent (PC) techniques and are mounted on the cold finger of a helium-flow cryostat at 10 K. The PC excitation source is a 150 W halogen lamp dispersed by a 0.25 m focal length monochromator, with an average excitation density of 100 $\mu W/cm^2$ (1×10^3 cm^{-2} carriers per period). The results show very clearly WSL's for all samples with a field dependence expected for the sample parameters. For the PL measurements we use a HeNe laser with an excitation intensity of about 100 mW/cm^2 and samples without electrical contacts.

The inset of Fig. 2(a) shows the PL spectra of sample 78 Å, which corresponds to the excitonic transition associated with the lower edge of the electron and hh miniband. Sample 78 Å has a broad PL line [full width at half maximum (FWHM) of 3 meV] indicating an inhomogeneous contribution to the broadening. The PL peak from sample 114 Å (not shown) has a width of 0.9 meV (FWHM) and can be well fitted with a Lorentzian shape, indicating that it is homogeneneously broadened. This observation is confirmed by experiments where the diffracted FWM signal is temporally resolved.[29]

Figure 2(a) shows a set of PC spectra for sample 78 Å, taken at different electric field strengths. Marked with lines as a guide to the eye are several el/hh and el/lh WS transitions. In the WS regime, el/hh transitions are observed for $n = -3, -2, ..., +1, +2$. Figure 2(b) shows a complete analysis of the peak positions. Their slopes are in excellent agreement with the sample parameters, as for all other samples. In contrast to sample 114 Å (data not shown; see, e.g., Ref. 31), we observe a more pronounced evolution of the miniband states to the WS regime. Even at a splitting of 20 meV, the absorption strength of the hh_0 and hh_{-1} transitions is comparable. This is expected for large minibandwidth samples due to the localization feature: the maximum observable splitting is given by the minibandwidth. We can also distinguish two el/lh ladders which we attribute to lh_{-1} and lh_{-2}. This is consistent with our calculations which suggest that these two transitions contain most of the oscillator strength for

TABLE I. Calculated minibandwidths of the different samples.

	Period				
Minibandwidth	78 Å	84 Å	97 Å	114 Å	128 Å
Δ_{el} (meV)	46	37	26	18	13
Δ_{hh} (meV)	4	2.8	1.9	1.2	0.9
Δ_{lh} (meV)	43	36	26	19	14

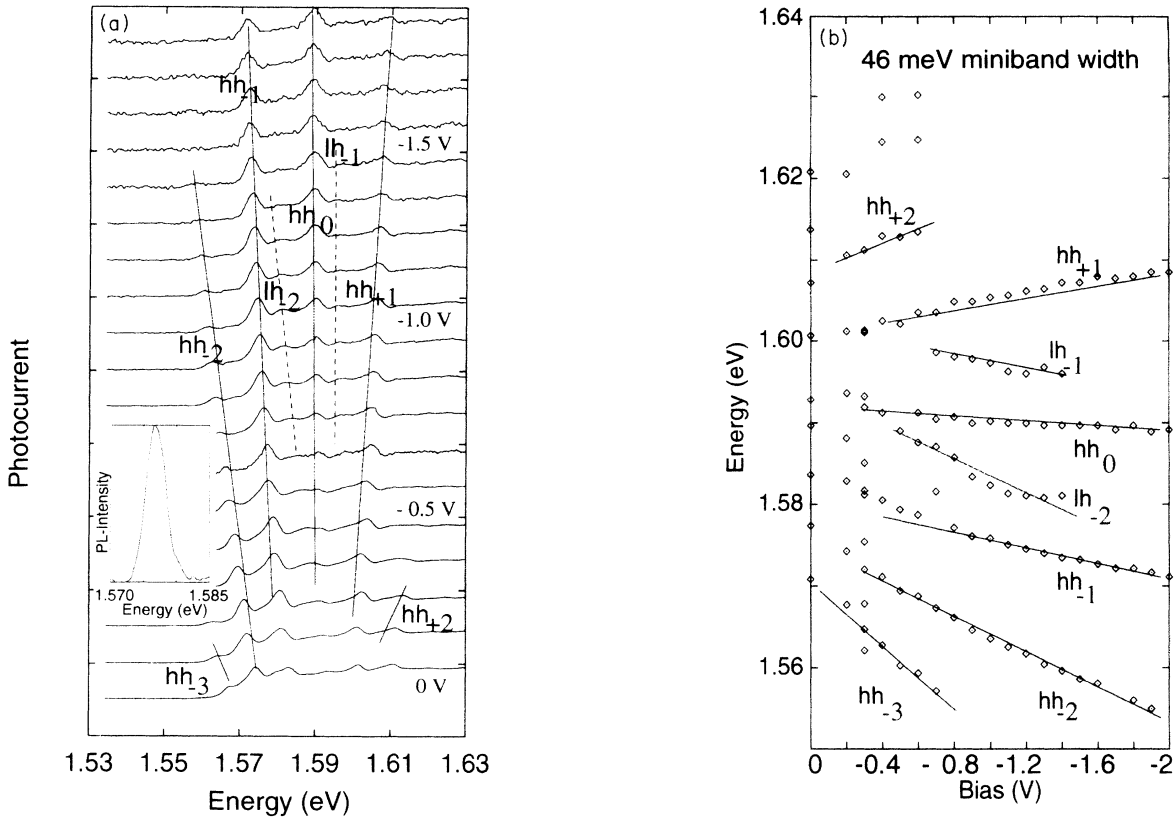

FIG. 2. (a) PC spectra for sample 78 Å at T =10 K for different electric field strengths. Several el/hh transitions are observed, indicated by solid lines. The inset shows the PL of the SL at 10 K, with a FWHM linewidth of 3 meV. (b) PC peak positions versus applied bias. Due to the larger minibandwidth, the localization is reduced with respect to sample 114 Å and the hh_{-3} to hh_{+2} WS transitions are visible. The ladder slopes agree very well with values corresponding to the nominal sample parameters.

fields above 25 kV/cm. Again in contrast to sample 114 Å, where the much weaker el/hh $2s$ transition can be resolved, there is no evidence of the $2s$ transitions. This is probably due to the enhanced oscillator strengths of the higher el/hh transitions. In the high-field regime of sample 114 Å we clearly observe the hh $1s$, hh $2s$, and lh $1s$ transitions (in energetic order). This classification is confirmed by a calculation of the transition energies, including excitonic effects.[35–37] The hh/lh splitting at high fields amounts to 11 meV, in contrast to the low-field regime with about 5.5 meV. The relative absorption strength in comparison to the el/hh transition is in good agreement with the theoretically expected 1:3 ratio.[14,38]

For the transient FWM experiments, we use a Kerr-lens mode-locked Ti:sapphire laser emitting 130 fs (FWHM) nearly transform-limited pulses. The transient optical experiments (see Fig. 3) are carried out in a standard two-beam copolarized degenerate FWM setup.[39] Detected is the time-integrated signal in the background-free direction $\vec{k}_3 = 2\vec{k}_2 - \vec{k}_1$. This signal in quantum wells is mainly governed by the exciton-exciton interaction, which leads to the evolution of a polarization wave.[40] The overall decay of the transient signal depending on the time delay τ for homogeneous broadening and non-interacting levels is given by[39]

$$I \propto \mu_{ij}^8 \exp\left(-\frac{2\tau}{T_2}\right) \tag{5}$$

with the interband matrix elements μ_{ij} according to Appendix B and the interband phase relaxation time T_2. The probability to observe the hh WS states in contrast to the lh WS states is strongly enhanced in a $\chi^{(3)}$ FWM experiment in contrast to linear experiments, due to the μ_{ij}^8 dependence. For inhomogeneous broadening, the diffracted signal is a photon echo occurring at $t = 2\tau$. The time-integrated signal then decays with a time constant that is 4 times smaller than the dephasing time, i.e., twice as fast as for the case of homogeneous broadening.

In our time-resolved measurements we use an excitation density of about 1×10^9 cm^{-2} carriers per period. At that density T_2 is not limited by carrier-carrier scattering, but we have to take into account strong static and dynamic screening effects in contrast to the cw experiments.

We observe large effects of field screening by the pho-

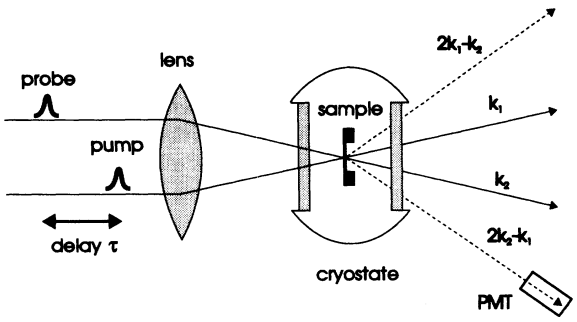

FIG. 3. Scheme of the self-diffracted FWM experiment. The two copolarized beams $\vec{k}_1$ and $\vec{k}_2$ are focused onto the sample, where they create a population grating. Detected is the time-integrated diffracted signal in the background-free direction $\vec{k}_3 = 2\vec{k}_2 - \vec{k}_1$ with a photomultiplier (PMT) as a function of the delay time τ.

toexcited carriers, which are attributed to the accumulation of carriers at the barriers at both ends of the SL due to the high repetition rate (76 MHz) of the laser. We measure the field screening by monitoring the actual field in the SL by the WS splitting and compare the bias voltage dependence of low-intensity cw photocurrent excitation to the pulsed excitation used in the transient experiments: For pulsed excitation, the WSL is measured by transmission spectroscopy with the broadband femtosecond laser pulse. Here we spectrally resolve the transmitted beam in the direction of $\vec{k}_1$ with a monochromator at time delay τ=0. Figure 4 shows the absorption of the WS levels computed from the transmission spectrum of the laser pulse. At flatband (+0.7 V) the hh and lh splitting of about 3 nm is clearly resolved. Under high excitation, the internal field stays near zero even for nonzero bias voltages (+0.7–0 V). Above a certain voltage threshold, the field starts to rise. The proportionality constant for this rise above the onset is identical to the constant observed for the low-level PC measurements (and, consequently, to that expected from the sample parameters). If the screening carriers would accumulate within the SL structure, i.e., produce an inhomogeneous screening, we would not observe sharp WS levels.

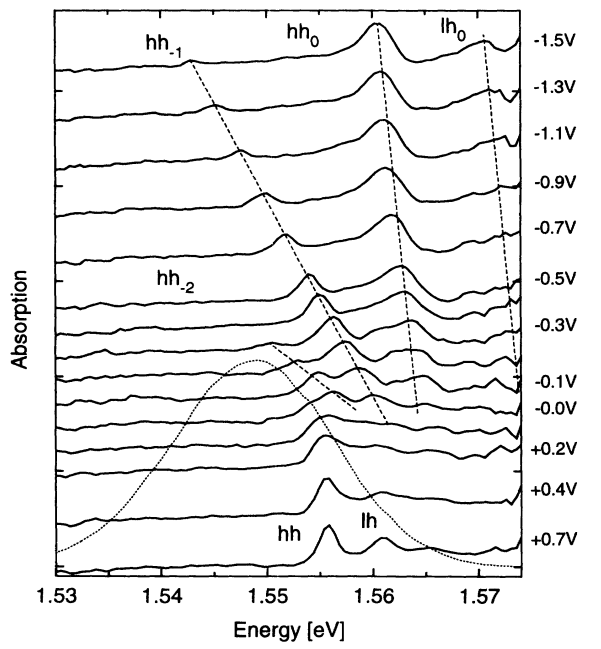

FIG. 4. WSL of sample 114 Å at 10 K. Plotted is the absorption, calculated from the transmission spectra of the broadband femtosecond pulse, as a function of the reverse bias voltage, for the same excitation density as in the time-resolved experiments. We calculate the offset out of the extrapolation of the hh_0 and hh_{-1} WS levels to zero splitting.

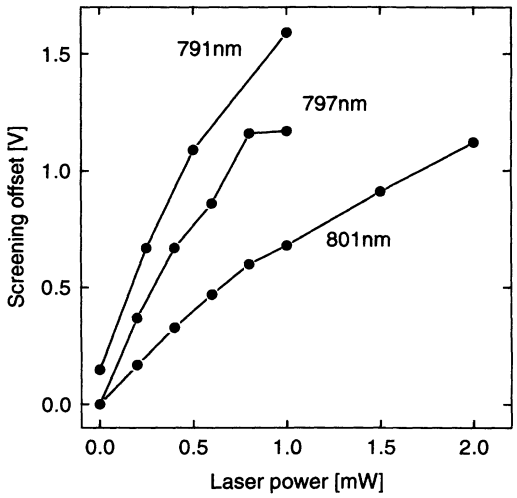

FIG. 5. Screening offset voltage for different intensities and different spectral peak positions of the exciting laser pulse. At a wavelength of 794 nm, the laser pulse would be centered at the hh_0 WS transition.

Figure 5 shows the dependence of the screening offset on the excitation conditions: The offset increases with intensity and is therefore dependent on the spectral position of the exciting laser pulse. The detailed dependence of the voltage threshold on temperature and sample parameters is discussed in Secs. IV and V.

With the same pump/probe setup transmission experiment we also obtain evidence for lateral transport of the photoexcited carrier distribution: If we move the probe beam away from the pump beam, we obtain an increase in the WS splitting, which is clear evidence for lateral inhomogenity of the internal electric field. To check for transients of the electric field, we varied the time delay between pump and probe. It turns out that the WS splitting depends only very weakly on the delay. We therefore speak of a quasistatic screening offset.

III. DEPENDENCE OF THE FWM SIGNAL ON THE APPLIED ELECTRIC FIELD

We start with the discussion of the transient FWM signals of the excited Bloch wave packets and its field

dependence: The bias field is changed from flatband to high applied voltages. Figure 6 shows the behavior of the FWM signal in a three-dimensional (3D) plot as a function of the time delay and the applied bias for the 114 Å sample. We observe three different regimes: (i) regime A from flatband at +0.7 V to about 0 V external field with a constant beating period; (ii) regime B with a period strongly depending on the applied bias; (iii) a high-field regime C, where we observe another beating with constant frequency (not shown in the 3D plot). Between regimes A and B, we observe a sharp decrease in the FWM amplitude.

The constant period of 830 fs in regime A is due to hh/lh beating. This conclusion is confirmed by the PC and femtosecond transmission spectroscopy (see Fig. 4). Due to the field screening, the regime A where virtually no internal field is present extends over about 1 V (+0.7 V to −0.3 V) of external bias voltage. At high fields (regime C), we observe a field-independent beating which is due to a superposition of the hh_0 and lh_0 levels, which contain most of the oscillator strength in the high-field regime. The beat period is about twice the flatband value, which is also reproduced in PC measurements and in good agreement with previous investigations of the exciton binding energy in SL.[22,41] This hh_0/lh_0 beating can also be observed at low applied fields if we tune the laser between the spectral position of hh_0 and lh_0 (see Fig. 13, wavelength 788 nm). The reason for the increase in the difference of the hh/lh excitonic binding energy is due to the localization effect: At flatband, a SL behaves more like a 3D system. The hh/lh transitions are centered at the miniband edges. With increasing electric field the wave functions become localized and therefore more two dimensional with the increased hh_0/lh_0 splitting of a single quantum well. The hh_0 and lh_0 states are now centered in the middle of the hh/lh miniband.

The decrease of the FWM amplitude between the field regimes A and B (the deep valley) is due to the rearrangements of the exciton binding energies in the transition regime from flatband to the WS regime. The FWM amplitude strongly depends on the excitonic interaction. In time-resolved experiments[42] we show that, in the deep valley, the interaction induced signal has its minimum and is increasing by increasing the field.

The dependence of the oscillation period in the regime B is inversely proportional to the field, as expected for the BO. The oscillations observed here are dominated by the hh WSL transitions, as the laser is positioned between the hh_{-1} and hh_0 transitions.

Figure 7 shows the FWM traces for different fields in a 2D semilogarithmic plot for sample 114 Å at 10 K. The internal field is here corrected for the field screening. At zero field we observe the hh/lh miniband beating with 830 fs, at the high field of 33 kV/cm the hh_0/lh_0 beating with about 450 fs. At intermediate field strengths the FWM traces clearly show up to ten oscillations of the wave packet in the mini Brillouin zone. A tuning range of one order of magnitude for the frequency is easily obtained. The asymmetric beating at low bias is due to the excitonic nonuniform splitting and a many-level superposition of the WS states, as the spectrum of the exciting laser pulse covers several of these states. This effect will be discussed in detail in Sec. VI. For a sample with the minibandwidth of 18 meV, the upper limit of the observed frequency is given by the time resolution of the laser pulse, the lower limit by the disappearance of the FWM signal and the sample quality.

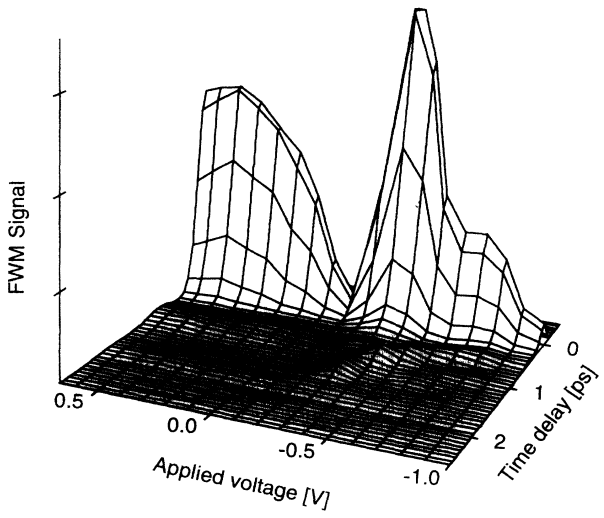

FIG. 6. 3D plot of the FWM signal as a function of delay time τ and applied external voltage. The oscillations with constant beating period at low bias are due to hh/lh beating, the oscillations at higher bias with decreasing period are due to BO.

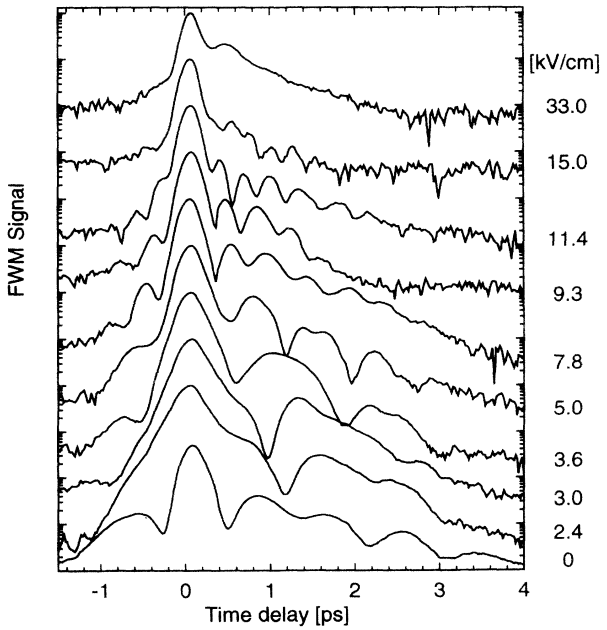

FIG. 7. Semilogarithmic plot of the FWM traces of sample 114 Å as a function of the delay time τ for various electric fields. The lattice temperature is 10 K, the excitation density about $1 \times 10^9 \mathrm{cm}^{-2}$ carriers per period.

To compare the data in the time domain to the BO theory, we extract the beating periods from Fig. 7 and calculate the corresponding energy splitting according to $\Delta E = h/\tau_B$. As shown in Fig. 8, the energy splitting is linearly dependent on the applied electric field (small deviations are due to excitonic effects and changes in the excitation density). The proportionality constant is in excellent agreement with the one expected from BO theory for the parameters of the SL as in the case of the PC spectra. This is clear evidence of one of the essential features of wave packets performing Bloch oscillations; therefore we assign the observed beating phenomena with Bloch oscillations.

Finally, we discuss the dependence of the overall dephasing time T_2 of the wave packets as a function of the applied field. Such a field dependence might give information about the onset of Zener tunneling:[5,10,11,43] There is a finite probability that the electron will tunnel into higher-energy bands, while reaching the upper band edge (this probability is neglected in the Houston approximation[2].)

Figure 9 shows T_2 as a function of the field, assuming homogeneous broadening. The data are obtained by analyzing the overall decay times of Fig. 7. For the hh/lh beating regime there is a systematic increase of T_2. This rise may be explained by better transport with increasing field (in contrast to shallow GaAs/$Al_xGa_{1-x}As$ quantum-wells,[44] where better transport reduces T_2). The screening electrons are no longer located in the wells but at the end of the SL structure. This could reduce the electron-electron scattering and thereby the phase relaxation time. In the BO regime (−0.3 to −1.5 V) there is no systematic dependence of the phase relaxation time on field, but it is reduced with respect to the hh/lh regime. Here we excite in the center of the miniband; therefore T_2 is reduced due to increasing scattering with free carriers generated in the continuum of energetic lower states. The "oscillations" of the decay times with the field are within the experimental error of the data. Up to quite high fields, no indication of a faster phase relaxation is visible. This is theoretically expected: The calculated times for Zener tunneling are one order of magnitude larger than one typical BO period.[10,43]

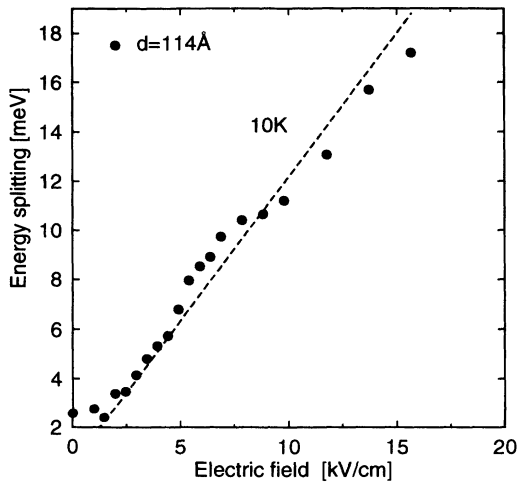

FIG. 8. Energy splitting $\Delta E = eFd$ calculated from the BO period using $\Delta E = h/\tau_B$ vs electric field at 10 K. The dashed line is a fit with a slope expected for the SL period of 114 Å.

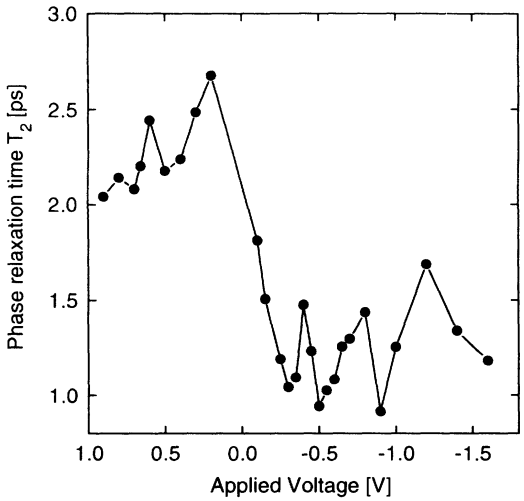

FIG. 9. Dependence of the phase relaxation time T_2 on the external applied voltage. The data are extracted from Fig. 7 using Eq. (5) and assuming a purely homogeneous broadening of the transition.

IV. DEPENDENCE OF BLOCH OSCILLATIONS AND hh/lh BEATS ON THE MINIBANDWIDTH

We study the dependence of the BO's on the miniband width for a number of reasons. The first two reasons address the question whether BO's can be observed in minibands with large width. (i) For obtaining BO's at room temperature, one needs rather large oscillation frequencies (larger than $\approx$ 5 THz) to compete with the phonon scattering. It is therefore necessary to use a large miniband width to overcome the localization effect to obtain such large frequencies. (ii) It is therefore also important to check whether there is a threshold effect when the miniband width exceeds the energy of the optical phonons. (iii) A third reason is the influence of the excitonic interaction on the formation of a WSL. It has been shown that the formation of WSL is suppressed for low miniband widths. The bandwidth needs to be larger than the exciton binding energy (5–10 meV).[45] There is no upper limit to the usable minibandwidth. In an experiment in a GaAs/AlAs with only one monolayer[20,24] barrier, a WSL was observed for a combined electron and hh minibandwidth of 380 meV.

In our experiments, we observe BO's and hh/lh beats in all the samples, with miniband widths from 13 to 46 meV. To compare the time-resolved data for the SL samples 84 and 128 Å to the BO theory, we extract the beating periods and calculate the corresponding energy splitting. The result is shown in Fig. 10: For both samples the

energy splitting depends linearly on the applied electric field (here the offset is corrected for the 10 K data). The proportionality constant is in excellent agreement with that expected from BO theory for the parameters of the different SL and at different temperatures. Increasing the temperature to 77 K increases the offset; this interesting feature will be discussed in detail in Sec. V.

The upper frequency limit of the oscillations for sample 128 Å is correlated to the minibandwidth: Due to localization effects of the electronic wave function, the maximum observable energy splitting for this sample with a 13 meV minibandwidth is limited to about 14 meV. Localization means that we are no longer able to excite a superposition of the hh_0 and hh_{-1} transitions and hence cannot excite a wave packet for BO's. This is an indirect confirmation of the second Bloch feature, the spatial oscillation. For sample 84 Å, the splitting is limited to the spectral width of the exciting laser pulse (18 meV). Using shorter laser pulses one should be able to observe Bloch frequencies up to 8 THz, according to the PC measurements and the minibandwidth of 37 meV of this particular sample. At that high frequency the BO should couple to the LO phonons. Additionally in the samples with minibandwidths larger than the LO phonon energy (about 36 meV) the BO electron could be scattered by the emission of a LO phonon at the upper band edge, even at 10 K: We do not observe any signs of a "phonon threshold," in contrast to Ref. 46. This scattering process would lead to a broadening of the WS levels corresponding to a larger minimal observable WS splitting. Nevertheless the sample design of Ref. 46 differs considerably from our samples. They use 100 periods of 30 Å wells and 30 Å barriers leading to a reduced sample quality. The minimum observable WS splitting in our FWM experiments, which principally can avoid the inhomogeneous broadening in contrast to linear cw experiments, depends in a complicated way on the sample quality (PL linewidth) and temperature. The splitting at 10 K varies from 2 meV for sample 114 Å to 5 meV for sample 78 Å at 10 K, shown in Figs. 8 and 10. The limiting process for T_2 at 10 K is therefore mainly due to interface scattering.

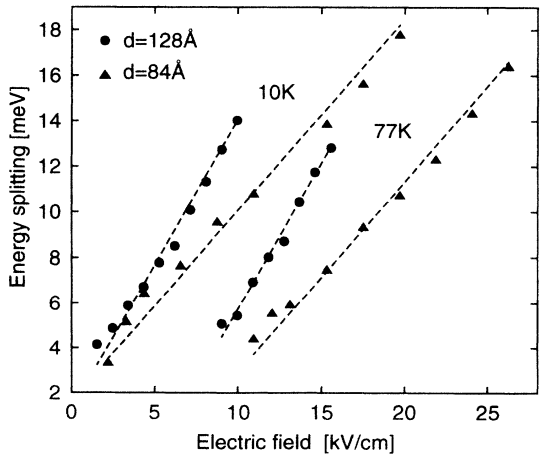

FIG. 10. Energy splitting $\Delta E = eFd$ calculated from the BO period using $\Delta E = h/\tau_B$ vs electric field at lattice temperatures of 10 K and 77 K. The dashed lines are fits with a slope expected for the SL period of 84 and 128 Å for the two different samples.

The hh/lh beating frequency has a maximum for sample 128 Å of 950 fs; for samples 78, 84, 97, and 114 Å it amounts to 660, 720, 790, and 830 fs, respectively. These experimental results are in contrast to Ref. 41. The different behavior is due to their sample design: They use equal well and barrier widths and approach bulk $Al_xGa_{1-x}As$ by decreasing the well/barrier width, i.e., increasing the minibandwidth. Therefore here the hh/lh splitting is decreasing with increasing minibandwidth. In our samples we approach bulk GaAs, with no corresponding hh/lh splitting, by increasing the well width with constant barrier width. Here increasing the minibandwidth increases the hh/lh splitting. With numerical calculations for the miniband positions according to Appendix A we estimate a maximum for the hh/lh splitting of 12 meV (beating period 300 fs) for 35 Å wells and 17 Å barriers. Further decreasing the well width with constant barrier width of 17 Å should decrease the hh/lh splitting like in Ref. 41.

Another crucial parameter strongly depending on the minibandwidth is the screening offset. The offset increases with the minibandwidth; this will be discussed in detail in Sec. V.

V. TEMPERATURE DEPENDENCE OF THE BLOCH OSCILLATIONS

For a possible application of the SL as a tunable tetrahertz emitter, it is crucial to work at room temperature, or at least at 77 K. The relevant damping process which limits the observation in our FWM experiments is the damping of the interband polarization $\rho^{(2)}$ associated with the excitonic el/hh wave packet. The interband phase relaxation time T_2 measured by FWM is strongly dependent on the lattice temperature. The corresponding intraband T_2 that governs the tetrahertz emission is at the same order of magnitude. Due to scattering with acoustic and optic phonons, T_2 decreases from several picoseconds at 10 K to 250 fs at room temperature.[47] The damping rate $\gamma = T_2^{-1}$ is given by

$$\gamma = \gamma_0 + \gamma_1 T + \gamma_2 \exp\left(-\frac{\hbar\omega_0}{kT}\right) \tag{6}$$

with typical parameters for high quality GaAs/$Al_xGa_{1-x}As$ heterostructures: γ_0=0.08 ps^{-1}, γ_1 =0.02 K^{-1} ps^{-1}, and γ_2=20.6 ps^{-1}. The scattering at interface roughnesses is included in γ_0. To allow at least one BO before the phase of the wave packet is lost, the condition $\tau_B < T_2$ must be fulfilled. For room temperature BO's, one would therefore need an oscillation frequency well above 4 THz.

Figure 11 shows the FWM traces for sample 84 Å at 77 K (the fields are corrected for the screening offset). Even at 77 K, four oscillations of the Bloch wave packet

are clearly visible; we observe BO's from 1.1 to 5 THz. At 10 K (data not shown), there are up to six oscillations visible, starting from 0.7 up to 5 THz. If we increase the temperature to 200 K we observe BO above 1.7 THz; at 300 K we do not observe BO's with 130 fs pulses. The lower limit is given for 77 and 200 K by the reduced T_2 due to LO phonon scattering, the upper limit by the time-resolution of our laser pulse. A close inspection of the data at 10 and 77 K reveals that the time constant T_2 for the exponential decay of the FWM signal and the exponential decay constant T_{BO} of the oscillation amplitude show a different temperature dependence: A careful fit to the 9.1 kV/cm data at 10 K and the 8.9 kV/cm data of Fig. 11 at 77 K reveals a decrease in T_2 from 1.5 ps to 0.75 ps in contrast to a decrease in T_{BO} from about 2.8 ps to 2.2 ps (assuming homogeneous broadening and a monoexponential decay of the oscillation amplitude). This indicates that the BO's are not damped by an interband homogeneous process, i.e., phonon scattering, which would become much faster going from 10 to 77 K, like the interband T_2, but by another effect. The damping due to the difference in the T_2 of the single WS transitions[48] would lead to a different temperature dependence. We believe therefore that the damping of the oscillation amplitude up to 100 K is mainly caused by a dephasing of the *wave packet* due to Coulomb interactions and interface scattering.

In the following, we discuss the temperature dependence of the screening offset for various miniband widths. Figure 12 displays the offset for samples 114 Å and 78 Å as a function of temperature. For the sample 114 Å with the smaller minibandwidth, the offset increases with temperature, with a maximum at 100 K. Above this temperature, it decreases strongly and finally becomes less than at 10 K. The sample 78 Å with the large minibandwidth has a much larger offset at 10 K. Above about 100 K, it decreases similarly to the other sample. All other samples show temperature dependences between these two cases.

At present, we have a qualitative, but not quantitative, understanding of these dependences. The increase of the offset in the 114 Å sample with temperature could be caused by less efficient vertical transport (i.e., in the growth direction) of the carriers due to thermal saturation of the miniband transport.[49] The decrease at higher temperatures could be caused by an onset of thermally activated transport across the barriers. The larger offset of the sample with the 46 meV minibandwidth at low temperature could be due to less effective transport caused by shorter transport scattering times: At low temperature and large minibandwidth (>10 meV) the transport scattering time is dominated by the elastic scattering time due to interface roughness.[50–55] Calculations of this scattering time reveal a strong dependence on the well width.[56,57] Sophisticated transport theories,[51,54] which take electron heating and different scattering times for inelastic (τ_{inel}) and elastic scattering (τ_{el}) into account, also show a strong dependence on the elastic scattering time. For the case of low temperature ($\Delta \gg kT$) and without electron heating the expression for the low field mobility μ is[55]

$$\mu = \frac{e\tau\Delta d^2}{2} \tag{7}$$

with the superlattice period d, $1/\tau = 1/\tau_{el} + 1/\tau_{inel}$, and the dependence:[56,57] $\tau_{el} \sim L_{well}^6$. With our experimental parameters (Δ=18 meV, L_{well}=97 Å and Δ=46 meV,

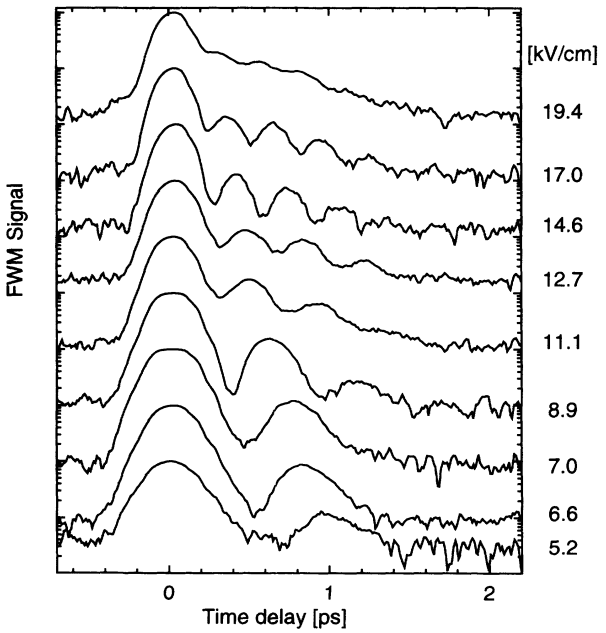

FIG. 11. Semilogarithmic plot of the FWM traces for sample 84 Å at 77 K as a function of the delay time, for various electric fields. Increasing the temperature decreases the phase relaxation time T_2. Even at this temperature four oscillations are clearly visible.

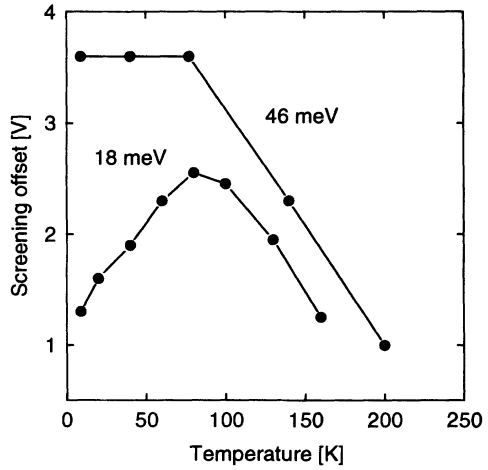

FIG. 12. Screening offset and its dependence on temperature and minibandwidth. For sample 114 Å with a minibandwidth of 18 meV (well width 97 Å), we obtain a maximum in the offset at about 100 K. Sample 78 Å with a miniband width of 46 meV (well width 61 Å) has a strongly increased offset at low temperature.

L_{well}=61 Å) we expect a large difference in the low-field mobilities.

As a measure for the quality of the interface we use the PL linewidth of the samples: The shape of the linewidth is closely related to the roughness of the interfaces[58,59] for $L_{well} < 100$ Å in single quantum wells. In our SL we attribute the broadening of the linewidth mainly to be due to interface scattering and not to well width fluctuations. This should be justified, as the broadening by interface scattering in high quality single quantum wells of 100 Å is at the order of 0.5 meV: This is predicted in theoretical calculations[60] and experimentally verified by us performing FWM measurements in single-quantum-well samples. The increase of the scattering time for the large miniband sample is thereby confirmed by the difference in the PL linewidths of the two samples: 0.9 meV for sample 114 Å and 3 meV for sample 78 Å. This is further supported by experiments with a perfect copy of sample 114 Å regarding the SL structure: The clone has a PL linewidth of 1.5 meV and shows a significant increase in the offset at 10 K of 0.5 V. A detailed quantitative understanding of these effects needs further experimental work.

VI. DEPENDENCE OF THE OSCILLATIONS ON THE EXCITATION CONDITIONS

The optical generation of WS wave packets in SL's provide large freedom to create wave packets with different weights and phases of the constituents. In this section, we discuss the dependence of the coherent dynamics of the oscillating wave packet on the excitation conditions. In particular, we demonstrate the existence of higher harmonics in the oscillations.

Depending on the spectral position of the broadband exciting laser pulse in the WSL, one can create wave packets of widely different shapes and dynamics. The most interesting is the coherent superposition of a symmetric set of electron WS states (e.g., −2, −1, 0, +1, and +2) with a pulse centered at the 0 transition. That would produce a breathing motion of the wave packet with no associated intraband dipole moment.[33] This simple picture has to be modified if we take the excitonic coupling of electrons and holes into account. Nevertheless, the main features of the wave packets are still preserved.

FWM experiments are not sensitive to the intraband polarization but to the third-order interband polarization (see Appendix B). Therefore we need no oscillating dipole moment of the Bloch frequency and are able to detect even a breathing motion. In this special case this breathing motion is closely connected to the occurrence of overtones. In this section we discuss therefore the observation of overtones: By changing the excitation energy, we observe partial recovery of the oscillating wave packet at integer fractions of the BO period. Figure 13 shows the measured time-integrated FWM traces for different spectral positions of the exciting laser pulse. Depending on the excitation conditions, the created wave packet oscillates either with the second or the fourth harmonic of the BO frequency τ_B of about 1.3 ps at a bias of 2.8 kV/cm. For a bias of 4 kV/cm ($\tau_B = 0.9$ ps) only the second harmonic and at 7 kV/cm ($\tau_B = 3.5$ ps) only the fundamental frequency are observed (data not shown).

In our experiments, we use 130 fs pulses corresponding to a spectral bandwidth of 18 meV. Therefore we are able to excite superpositions of more than five WS states: The energy splitting between two adjacent states is about $\Delta E = eFd = h/\tau_B$=3.2 meV, with an applied electric field F of 2.8 kV/cm and a lattice period d of 114 Å. By varying the spectral position of the laser pulse, we choose different weightings of the superimposed levels in the wave packet. A superposition of states, separated by ΔE, $2\Delta E$, $3\Delta E$, and $4\Delta E$, will therefore have at least some oscillating contributions with τ_B, $\tau_B/2$, $\tau_B/3$, and $\tau_B/4$.

To give a precise theoretical description of this dynamical behavior of the wave packet according to Eq. (4), we calculate the field-dependent absorption strength of the WS states (see Fig. 14), neglecting the Coulomb interaction between electron and hole. The excitonic coupling does not change the absorption strengths qualitatively; there is only a quantitative shift in the strength.[35] We use a numerical calculation of the envelope wave function in a finite SL since the WS wave functions are not a good approximation: This approximation fails at low bias for the electrons[61] and is even insufficient over the entire bias range for the holes, due to the failure of the tight-binding model. A corresponding calculation with WS states would therefore not reproduce the asymmetry

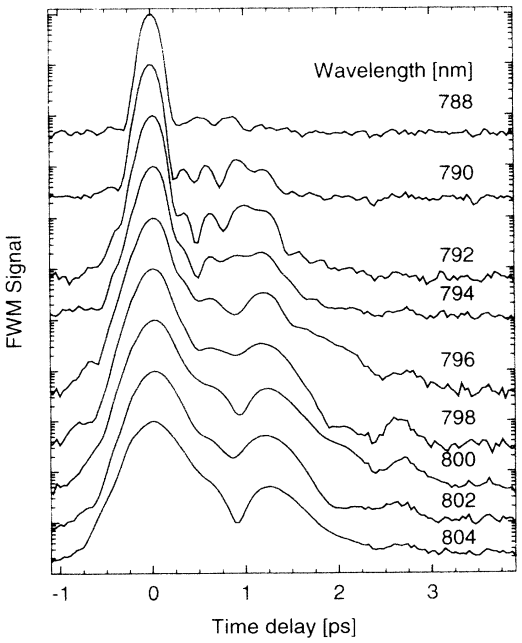

FIG. 13. Time-integrated FWM signal at 10 K for various spectral positions of the femtosecond laser pulse (from 788 to 804 nm). The applied electric field and the excitation density are kept constant. The fourth harmonic of $\tau_B/4$ evolves out of the fundamental BO period of τ_B=1.3 ps if the laser is tuned between the hh_{-2} and hh_{+2} WS levels at shorter wavelengths.

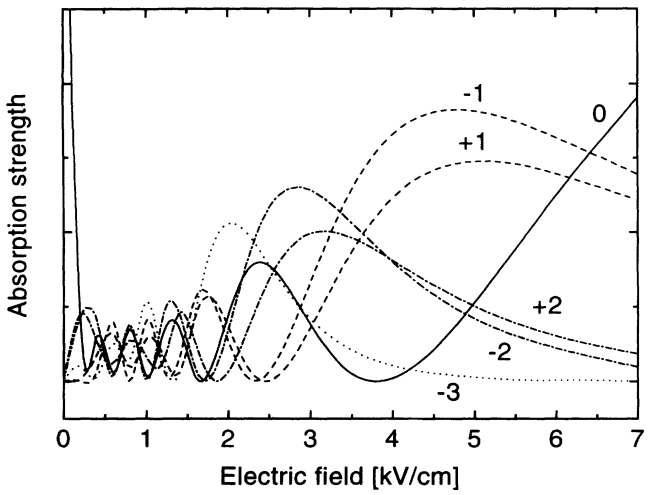

FIG. 14. Numerically calculated field dependence of the absorption strength for the el/hh WS states -3, -2, -1, 0, $+1$ and $+2$ in a superlattice of 19 quantum wells. The asymmetry in the absorption for the positive and negative WSL at low bias is not reproduced in the WS model.

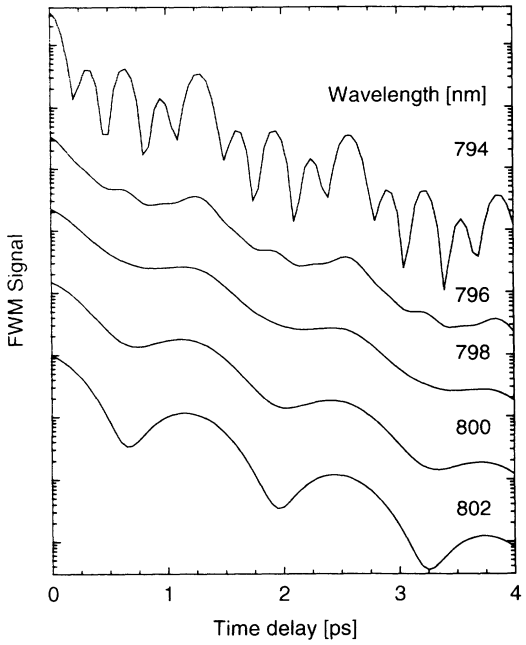

FIG. 15. Semilogarithmic plot of the calculated FWM traces according to Appendix B for an electric field of 2.8 kV/cm. The wavelength labels the peak position of the spectral position of the Gaussian shaped exciting laser pulse. At the wavelength 794 nm the pulse is centered at the hh_0 WS transition. The fourth harmonic is clearly visible at this spectral position.

in the absorption of negative/positive WS transitions. Since the wave function is already localized within about 10 periods at a bias of 3 kV/cm, we use only a 19 period SL. The wave functions are obtained with a modified Numerov algorithm as described in Appendix A. The absorption strength is proportional to the square of the el/hh transition-matrix element. In the bias field regime between 2 and 3 kV/cm, most of the absorption strength is concentrated in the hh_{-2} and hh_{+2} transitions, less in the hh_{-1}, hh_0, and hh_{+1} transitions. This disappearance of the central transitions of the WSL for certain fields has previously been observed experimentally.[19] We can thus excite a wave packet in which the hh_{-2} and hh_{+2} transitions have the largest fraction, which is the prerequisite for the clear observation of the fourth harmonic. At a bias of 4 kV/cm all absorption strength is concentrated in the hh_{-1} and hh_{+1} transitions, leading to the observation of the second harmonic. Above 6 kV/cm the hh_0 transition gains most of the absorption strength and only the fundamental BO frequency is visible.

With the calculated oscillator strengths as input, we theoretically model our FWM data with a noninteracting third-order density-matrix theory for a many-level system[39,48] (discussed in detail in Appendix B). For the calculated FWM traces of Fig. 15, we include the spectral weight of the 18 meV Gaussian laser shape. If the laser is positioned directly onto the hh_0 transition, we get a strong modulation with the fourth harmonic of the BO frequency. Even with the assumption of an evenly spaced WSL and equal damping constants γ_{ij} for all transitions, good qualitative agreement between experiment and theory is obtained.

It is important to point out that the FWM technique used here shows a quite different response to the wave-packet structure than linear techniques: The calculated interband absorption coefficients affect the weighting of the WS levels and therefore the oscillating parts in the FWM signal in the fourth power (see Appendix B). Therefore, in the interband $\chi^{(3)}$ experiment (i.e., FWM), the possibility of observing these overtones is enhanced in contrast to an intraband experiment (e.g., transmittive electro-optic sampling[29,30] and tetrahertz emission[31]).

VII. SPECTRAL RESOLUTION OF THE DIFFRACTED SIGNAL: QUANTUM VS POLARIZATION INTERFERENCE

The coherent optical excitation of a number of optical transitions with a broadband pulse can lead to two different oscillation phenomena observed in the field radiated by the system: The most simple mechanism is the far-field interference of radiators with slightly different frequency, as observed, e.g., in quantum-well samples with regions of slightly different thickness.[62] The oscillation is then caused by the interference of two or more independent two-level systems. A different mechanism, which is discussed in this article, is the oscillation of the dipole moment caused by a quantum-mechanical superposition of eigenstates by optical transitions from a common ground state. Such interference has been termed *quantum beats*. The experimental results by time-integrated FWM (Refs. 25 and 26) and tetrahertz emission[31] about BO's presented up to now have not

given experimental evidence that indeed quantum interference is involved, as should be the case for BO: In the time integrated FWM experiments, polarization and quantum interference give the same signal shape.[63] The tetrahertz signals could also be explained by a nonlinear difference frequency mixing of two polarizations by a $\chi^{(2)}$ process.

In the FWM experiment we use the fact that the $\chi^{(3)}$ signal, which is due to interference terms of $\chi^{(1)}$ polarizations contains information about the origin of the interference. It has been shown that two possibilities for an experimental distinction between quantum beats and polarization beats exist: time resolving[64] or spectrally resolving[65] the diffracted signal.

We spectrally resolve the FWM signal to verify that we really observe quantum interference. For this purpose we put the monochromator in the direction $\vec{k}_3$ of the diffracted signal, between the sample and the photomultiplier. The resolution of the monochromator we use in the experiment is about 2 nm. One expects different beating behavior in the spectrally resolved FWM signal for quantum beats and polarization interference:[65] For quantum beats, the oscillations have the same phase for all frequencies; for polarization interference, the phase oscillates between 0 and π. Our experiments clearly show quantum interference (Fig. 16): The phase of the oscillations between the single oscillators is independent of the frequency, as predicted for BO's. As one would expect, the spectral distance of the oscillators of about 2.6 nm corresponds to the BO period of 830 fs on the delay time axis. The oscillators are at the low applied field of 4.4 kV/cm due to excitonic effects not completely equidistant.

The quantum interference nature of BO's is further corroborated by theoretically modeling the experiment. We evaluate Eq. (B4) for a four-level system (one common ground state and three excited WS states) with equal weighting, but do not include a convolution with the spectrometer transmission function before taking the square of the polarization.

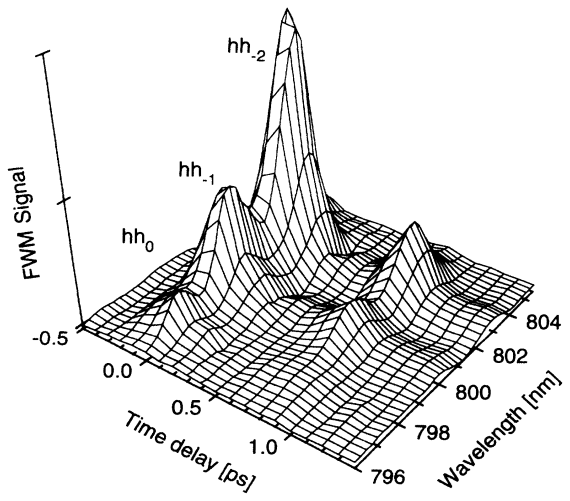

FIG. 16. Spectrally resolved FWM signal for sample 114 Å versus time delay for an applied field of 4.4 kV/cm. With the spectral position (801 nm) of the 18 meV wide pulse, the hh_{-2}, hh_{-1}, and hh_0 transitions are excited. The data are not corrected for the spectral shape of the laser pulse.

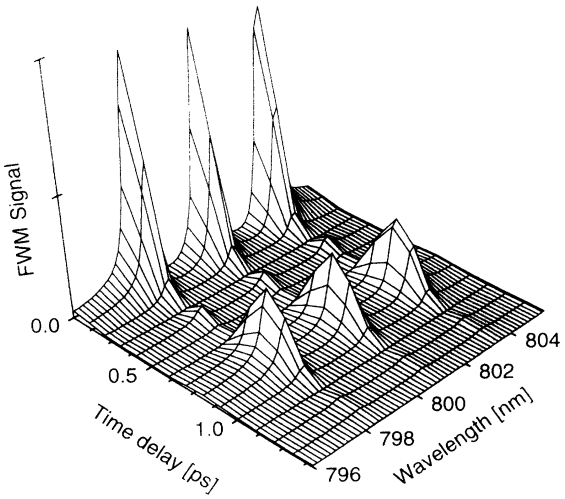

FIG. 17. Calculated spectrally resolved FWM signal according to Appendix B for the case of quantum beats. The phase relaxation time T_2 of 1.4 ps and the electric field of 4.4 kV/cm are extracted out of Fig. 16. The agreement between the theoretical calculations and the experimental data is excellent. In both experiment and theory no phase shift between the single oscillators is visible.

The phase relaxation time T_2 of 1.4 ps was extracted from the exponential decay of the experimental data in Fig. 16, assuming a purely homogeneous broadening. The result is shown in Fig. 17. Note that the experimental data are not corrected for the spectral intensity profile of the laser pulse, which is centered at 801 nm. Additionally the peaks are broadened due to the limited resolution of the monochromator. Thus the relative amplitude and width of the peaks is different in experiment and theory. The behavior of the oscillation structure, however, agrees very well and confirms the observation of quantum beats.

VIII. CONCLUSIONS

We have presented a comprehensive study of Bloch oscillations and heavy/light-hole beats in high quality $GaAs/Al_xGa_{1-x}As$ semiconductor superlattices. This study demonstrates the realization of an important theoretical concept in solid state physics and gives a variety of design considerations for future room temperature device applications. In samples well characterized by cw photocurrent and femtosecond-transmission spectroscopy a pronounced Wannier-Stark ladder is observed at excitation densities between 1×10^3 and 1×10^9 cm^{-2} carriers per period. The experimental observable minimum Wannier-Stark splitting at 10 K depends on the quality of the superlattice, which is mainly determined by the photoluminescence linewidth. In all transient four-wave

mixing experiments performed we observe significant oscillations on the decay of the signal, strongly depending on the applied electric field. The linear dependence of the oscillation period at intermediate fields is in excellent agreement with the behavior expected from Bloch oscillations. The oscillations at flatband and high fields are due to heavy/light-hole beats. The tuning range of the Bloch oscillations frequency covers the regime from 0.5 to 5 THz; they are observed up to 200 K. The lower limit is strongly dependent on the phase relaxation time T_2; the upper limit is due to the minibandwidth or time resolution of the laser pulse. At 10 K the T_2 is dominated by interface scattering, above 77 K by phonon scattering. We have no evidence of a field dependence of T_2 due to Zener tunneling and a significantly enhanced LO phonon scattering rate for a minibandwidth above 36 meV. In all field regimes the four-wave mixing amplitude is governed by excitonic interactions. By spectrally resolving the four-wave mixing signal we proved that these oscillations are caused by quantum-beat interference of Wannier-Stark levels. When investigating the Bloch oscillations, we notice a peculiar dependence of the field in the sample on the external bias voltage caused by the field screening due to the photoexcited carriers. By a careful measurement of the cw optical properties under pulsed excitation, we eliminate the influence of this effect in our Bloch oscillation study. Nevertheless, these screening effects are interesting by themselves and need further experimental and theoretical investigation.

In some carefully designed experiments the *optical control* of excited wave packets is demonstrated. By a variation of the excitation energy, wave packets with completely different shape and oscillatory motion can be created. The observation of higher harmonics indicates the coherent superposition of more than five Wannier-Stark states. This was confirmed by an excellent agreement between the experiment and theoretical calculations.

ACKNOWLEDGMENTS

We gratefully acknowledge valuable and stimulating discussions with D. Dunlap, M. Dignam, H.G. Roskos, J. Shah, and H.J. Bakker. We thank K. Victor for the discussion of the cw photocurrent spectra and C. Waschke for the help with the screening studies. This work has been supported by the Deutsche Forschungsgemeinschaft.

APPENDIX A: MODIFIED NUMEROV ALGORITHM

We calculate the wave functions and their eigenenergies by solving numerically the Schrödinger equation for the envelope wave function. Therefore we obtain reliable wave functions even at low applied bias, where the WS approach is no longer valid.[61] The calculation is done using a modified Numerov algorithm. The usual form of this algorithm[66] does not take into account the different mass of electrons and holes in well and barrier, but only the potential difference. According to Ref. 67, we write the operator for the kinetic energy with $m(z)$ a piecewise constant:

$$T = -\frac{\hbar^2}{2}\frac{\partial}{\partial z}\frac{1}{m(z)}\frac{\partial}{\partial z} \tag{A1}$$

with the boundary conditions for the wave function Ψ and its derivative Ψ':

$$\Psi_+ = \Psi_- \quad \text{and} \quad \frac{\Psi'_+}{m_+} = \frac{\Psi'_-}{m_-}, \tag{A2}$$

where + and − denote the left- and the right-hand side of the boundary, respectively. We can include the mass difference by writing the following equation for the envelope wave function in the z direction:

$$\frac{\partial}{\partial z}\frac{1}{m(z)}\frac{\partial}{\partial z}\Psi(z) + \frac{2}{\hbar^2}[E - V(z)]\Psi(z) = 0\ . \tag{A3}$$

With a Taylor expansion in $z_{i+1} - z_i = \Delta z$ up to the fourth order and a piecewise constant $V(z) \to V_i, m(z) \to m_i$, we get the expression

$$\Psi_{i+1} = \left(\frac{2(\Delta z)^2 m_i}{\hbar^2}(V_i - E) + \frac{m_i}{m_{i-1}} + 1\right)\Psi_i - \frac{m_i}{m_{i-1}}\Psi_{i-1}. \tag{A4}$$

For the case of equal masses, we obtain the well known Numerov algorithm.[66] For energy eigenvalues this iteration will converge; otherwise it will diverge. The algorithm does not include the Coulomb interaction between electrons and holes. It is about 10 times faster than the transfer-matrix method and in excellent agreement with Kronig-Penney calculations for the minibandwidth at flatband.

We use the following material parameters,[14,68] and do not include the k-space dependence of the effective masses:

$$\begin{aligned} E_{\text{gap}}(10\text{ K}) &= 1.520 + 1.247x, \\ M_{\text{el}}(\text{Al}_x\text{Ga}_{1-x}\text{As}) &= 0.067 + 0.083x, \\ M_{\text{hh}}(\text{Al}_x\text{Ga}_{1-x}\text{As}) &= 0.380 + 0.310x, \\ M_{\text{lh}}(\text{Al}_x\text{Ga}_{1-x}\text{As}) &= 0.087 + 0.063x. \end{aligned} \tag{A5}$$

For the conduction/valence-band offsets, we use the now commonly accepted 65:35 ratio.[14,69]

APPENDIX B: THIRD-ORDER DENSITY-MATRIX FORMALISM FOR A MANY-LEVEL SYSTEM

For a calculation of the time evolution of the FWM signal in a biased SL, one can apply different theoretical concepts. In an approach close to the semiclassical picture in k space, von Plessen and Thomas[12] calculated the FWM signal using a time evolution operator. This theory uses equal and field-independent transition probabilities for each of the different transitions in k space from the valence band to the conducting band.

We apply the theoretical model given in Ref. 48 to a many-level system, i.e., the WSL. The WSL is described as a noninteracting homogeneously broadened many-level system with a single common ground state. In the WS picture, we can easily include different and field-dependent transition-matrix elements μ_{jk} for each level. We use a common time delay convention: The delay time τ is positive if pulse 1 interacts before pulse 2 with the sample. For simple analytic expressions, we restrict ourselves to the case of equal spacing of the WSL and the same $\gamma = 1/T_2$ for every WS level. Denoting $\Omega_{0k} = \omega_{0k} - i\gamma_{0k}$, with $k = 0, \pm 1, \pm 2, \ldots$, we get the following expression for a many-level quantum-beat interference and $\delta(t+\tau)/\delta(t)$ shaped excitation pulses:

$$\vec{P}^{(3)}_{2\vec{k}_2-\vec{k}_1}(t,\tau) = \Theta(t)\Theta(\tau)\sum_{k,j}\mu_{0j}^2\mu_{0k}^2 \times \exp(-i\Omega_{0j}t)\exp(i\Omega_{0k}\tau) \tag{B1}$$

with $\omega_{0k} = \omega_0 + k\Delta\omega$, $\Delta\omega = eFd/\hbar$, and $\gamma_{0j} = \gamma_{0k} = \gamma$ and

$$\vec{P}^{(3)}_{2\vec{k}_2-\vec{k}_1}(t,\tau) = \Theta(t)\Theta(\tau)\exp[-\gamma(t+\tau)]\exp[-i\omega_0(t-\tau)] \times \sum_k \mu_{0k}^2 \exp(-i\Delta\omega k t) \times \sum_k \mu_{0k}^2 \exp(i\Delta\omega k\tau). \tag{B2}$$

Note that this formula is "symmetric" in the time t and the delay τ. It is separable regarding these two variables. In the time-resolved measurements, we detect the intensity of the light emitted by $\vec{P}^{(3)}$ in the direction of $\vec{k}_3 = 2\vec{k}_2 - \vec{k}_1$:

$$|\vec{P}^{(3)}_{2\vec{k}_2-\vec{k}_1}(t,\tau)|^2 = \Theta(t)\Theta(\tau)\exp[-2\gamma(t+\tau)]\left(\sum_k \mu_{0k}^4 + \sum_{k>j} 2\mu_{0j}^2\mu_{0k}^2\cos[\Delta\omega(k-j)\tau]\right) \times \left(\sum_k \mu_{0k}^4 + \sum_{k>j} 2\mu_{0j}^2\mu_{0k}^2\cos[\Delta\omega(k-j)t]\right). \tag{B3}$$

As a function of delay time, we observe the behavior as discussed in Ref. 64 for the case of equal γ_{0k}, in contrast to the results of Ref. 70.

To interpret the spectrally resolved measurements, a Fourier transform[70] of Eq. (B2) before taking the square of the polarization yields

$$\left|P^{(3)}_{2\vec{k}_2-\vec{k}_1}(w,\tau)\right|^2 = \Theta(\tau)\exp(-2\gamma\tau)\left|\sum_k \mu_{0k}^2\exp(i\Delta\omega k\tau)\sum_k \frac{\mu_{0k}^2}{(\omega_0 + k\Delta\omega - \omega) - i\gamma}\right|^2. \tag{B4}$$

[1] F. Bloch, Z. Phys. **52**, 555 (1928).
[2] W.V. Houston, Phys. Rev. **57**, 184 (1940).
[3] N. Ashcroft and D. Mermin, *Solid State Physics*, 1st ed. (CBS Publishing Asia LTD, Ithaca, 1988), pp. 224 and 225.
[4] L. Esaki and R. Tsu, IBM J. Res. Dev. **61**, 61 (1970).
[5] C. Zener, Proc. R. Soc. London Ser. A **145**, 523 (1934).
[6] L.V. Keldysh, Zh. Eksp. Teor. Fiz. **34**, 1138 (1958) [Sov. Phys. JETP **34**, 788 (1958)].
[7] G.H. Wannier, Rev. Mod. Phys. **34**, 645 (1962).

[8] H.N. Nazareno and J.C. Gallardo, Phys. Status Solidi B **153**, 179 (1989).
[9] G. Bastard, and R. Ferreira, in *Spectroscopy of Semiconductor Microstructures*, Vol. 206 of *NATO Advanced Study Institute, Series B: Physics*, edited by G. Fasol and A. Fasolini (Plenum Press, New York, 1989), p. 333.
[10] J.B. Krieger and G.J. Iafrate, Phys. Rev. B **33**, 5494 (1986).
[11] G. Nenciu, Rev. Mod. Phys. **63**, 91 (1991).
[12] G. von Plessen and P. Thomas, Phys. Rev. B **45**, 9185 (1992).
[13] W. Franz, Z. Naturforsch. Teil A **13**, 1958 (1958).
[14] D.A.B. Miller, D.S. Chemla, T.C. Damen, A.C. Gossard, W. Wiegmann, T.H. Wood, and C.A. Burrus, Phys. Rev. B **32**, 1043 (1985).
[15] L. Schultheis and J. Hegarty, J. Phys. (Paris) Colloq. **46**, C7-167 (1985); L. Schultheis, J.Kuhl, and A. Honold, Phys. Rev. Lett. **57**, 1635 (1986).
[16] F. Agulló-Rueda, E.E. Mendez, and J.M. Hong, Phys. Rev. B **40**, 1357 (1989).
[17] E.E. Mendez, F. Agulló-Rueda, and J.M. Hong, Phys. Rev. Lett. **60**, 2426 (1988).
[18] P. Voisin, J. Bleuse, C. Bouche, S. Gaillard, C. Alibert, and A. Regreny, Phys. Rev. Lett. **61**, 1639 (1988).
[19] E.E. Mendez, F. Agulló-Rueda, and J.M. Hong, Appl. Phys. Lett. **56**, 2545 (1990).
[20] K.H. Schmidt, W. Geißelbrecht, N. Linder, D.H. Döhler, H.T. Grahn, K. Ploog, and H. Schneider, in Proceedings of the Sixth International Conference on Modulated Semiconductor Structures [Solid State Electron. **37**, 1337 (1994)].
[21] A. Sibille, J.F. Palmier, and F. Mollot, Appl. Phys. Lett. **60**, 457 (1992).
[22] F. Agulló-Rueda, J.A. Brum, E.E. Mendez, and J.M. Hong, Phys. Rev. B **41**, 1676 (1990).
[23] M.M. Dignam and J.E. Sipe, Phys. Rev. Lett. **64**, 1797 (1990).
[24] H. Schneider, A. Fischer, and K. Ploog, Phys. Rev. B **45**, 6329 (1992).
[25] J. Feldmann, K. Leo, J. Shah, D.A.B. Miller, J. E. Cunningham, S. Schmitt-Rink, T. Meier, G. von Plessen, A. Schulze, and P. Thomas, Phys. Rev. B **46**, 7252 (1992).
[26] K. Leo, P. Haring Bolivar, F. Brüggemann, R. Schwedler, and K. Köhler, Solid State Commun. **84**, 943 (1992).
[27] P. Leisching, C. Waschke, P. Haring Bolivar, W. Beck, H.G. Roskos, K. Leo, H. Kurz, and K. Köhler, in *International Semiconductor Device Research Symposium* (University of Virginia, Charlottesville, VA, 1993), p. 85.
[28] P. Leisching, C. Waschke, W. Beck, P. Haring Bolivar, H.G. Roskos, K. Leo, H. Kurz, and K. Köhler, in *Coherent Optical Interactions in Semiconductors*, Vol. 330 of *NATO Advanced Study Institute, Series B: Physics*, edited by R. T. Phillips (Plenum Press, New York, 1994), pp. 325–329.
[29] P. Leisching, T. Dekorsy, C. Waschke, W. Beck, H.G. Roskos, K. Leo, H. Kurz, and K. Köhler, in *Ultrafast Phenomenon IX*, edited by G. Mourou, A. Zewail, P. Barbara, and W. Knox, Springer Series in Chemical Physics Vol. 60 (Springer-Verlag, Berlin, 1994).
[30] T. Dekorsy, P. Leisching, K. Leo, H. Kurz, and K. Köhler, Phys. Rev. B **50**, 8106 (1994).
[31] C. Waschke, H.G. Roskos, R. Schwedler, K. Leo, H. Kurz, and K. Köhler, Phys. Rev. Lett. **70**, 3319 (1993).
[32] C. Waschke, P. Leisching, P. Haring Boliviar, R. Schwedler, F. Brüggemann, H.G. Roskos, K. Leo, H. Kurz, and K. Köhler, Solid State Electron. **37**, 1321 (1994).
[33] M.M. Dignam, J.E. Sipe, and J. Shah, Phys. Rev. B **49**, 10 502 (1994).
[34] A.M. Bouchard and M. Luban, Phys. Rev. B **47**, 6815 (1993).
[35] K. Victor (private communication).
[36] P. Lefebvre, P. Christol, and H. Mathieu, Phys. Rev. B **48**, 17 308 (1993).
[37] P. Lefebvre, P. Christol, and H. Mathieu, J. Phys. IV **3**, C5-377 (1993).
[38] R.C. Miller and D.A. Kleinman, J. Lumin. **30**, 520 (1985).
[39] T. Yajima and Y. Taira, J. Opt. Soc. Jpn. **47**, 1620 (1979).
[40] K. Leo, M. Wegener, J. Shah, D.S. Chemla, E.O. Göbel, T.C. Damen, S. Schmitt-Rink, and W. Schäfer, Phys. Rev. Lett. **65**, 1340 (1990).
[41] A. Chomette, B. Lambert, B. Deveaud, F. Clerot, A. Regreny, and G. Bastard, Europhys. Lett. **4**, 461 (1987).
[42] P. Leisching, W. Beck, K. Leo, H. Kurz, W. Schäfer, and K. Köhler (unpublished).
[43] A. Di Carlo, P. Vogl, and W. Pötz, Phys. Rev. B (to be published).
[44] G. von Plessen, J. Feldmann, E.O. Göbel, K.W. Goossen, D.A.B. Miller, and J.E. Cunningham, Appl. Phys. Lett. **63**, 2372 (1993).
[45] A.M. Fox, D.A.B. Miller, J.E. Cunningham, W.Y. Jan, C.Y. Chao, and S.L. Chuang, Phys. Rev. B **44**, 6231 (1991).
[46] G. von Plessen, T. Meier, J. Feldmann, E.O. Göbel, and P. Thomas, Phys. Rev. B **49**, 14 058 (1994).
[47] K. Leo, P. Haring Bolivar, G. Maidorn, H. Kurz, and K. Köhler, in *Physics of Semiconductors*, edited by Ping Jiang and Hou-Zhi Zheng (World Scientific, Singapore, 1993), p. 983.
[48] S. Schmitt-Rink, D. Bennhardt, V. Heuckeroth, P. Thomas, P. Haring, G. Maidorn, H. J. Bakker, K. Leo, D.S. Kim, J. Shah, and K. Köhler, Phys. Rev. B **46**, 10 460 (1992).
[49] G. Brozak, M. Helm, F. DeRosa, C.H. Perry, M. Kozak, R. Bhat, and S.J. Allen, Phys. Rev. Lett. **64**, 3163 (1990).
[50] J.F. Palmier, G. Etemadi, A. Sibille, M. Hadjazi, F. Mollot, and R. Planel, Surf. Sci. **267**, 574 (1992).
[51] X.L. Lei and I.C. da Cunha Lima, J. Appl. Phys. **71**, 5517 (1992).
[52] A. Sibille, J.F. Palmier, M. Hadjazi, H. Wang, G. Etemadi, E. Dutisseuil, and F. Mollot, Superlatt. Microstruct. **13**, 247 (1993).
[53] F. Piazza, L. Pavesi, A. Vinattieri, J. Martinez-Pastor, and M. Colocci, Phys. Rev. B **47**, 10 625 (1993).
[54] C. Minot, H. Le Person, J.F. Palmier, N. Sahri, F. Mollot, and R. Planel, Semicond. Sci. Technol. **9**, 789 (1994).
[55] R.A. Suris and B.S. Shchamkhalova, Fiz. Tekh. Poluprovodn. **18**, 1178 (1984) [Sov. Phys. Semicond. **18**, 738 (1984)].
[56] R. Ferreira and G. Bastard, Phys. Rev. B **40**, 1074 (1989).
[57] I. Dharssi and P.N. Butcher, J. Phys. Condens. Matter **2**, 4629 (1990).
[58] J. Singh, K.K. Bajaj, and S. Chaudhuri, Appl. Phys. Lett. **44**, 805 (1984).
[59] M. Tanaka, and H. Sakaki, J. Cryst. Growth **81**, 153 (1987).
[60] T. Takagahara, Phys. Rev. B **32**, 7013 (1985).
[61] J. Bleuse, G. Bastard, and P. Voisin, Phys. Rev. Lett. **60**, 220 (1988).
[62] E.O. Göbel, K. Leo, T.C. Damen, J. Shah, S. Schmitt-Rink, W. Schäfer, J.F. Müller, and K. Köhler, Phys. Rev. Lett. **64**, 1801 (1990).

[63] K. Leo, E.O. Göbel, T.C. Damen, J. Shah, S. Schmitt-Rink, W. Schäfer, J.F. Müller, K. Köhler, and P. Ganser, Phys. Rev. B **44**, 5726 (1991).
[64] M. Koch, J. Feldmann, G. von Plessen, E.O. Göbel, and P. Thomas, Phys. Rev. Lett. **69**, 3631 (1992).
[65] T. Tokizaki, A. Nakamura, Y. Ishida, T. Yaijma, I. Akai, and T. Karasawa, in *Ultrafast Phenomena VII*, edited by C. B. Harris, E. P. Ippen, G. A. Mourou, and A. H. Zewail Springer Series in Chemical Physics Vol. 53 (Springer-Verlag, Berlin, 1990), p. 253.
[66] J.P. Killingbeck, *Microcomputer Quantum Mechanics* (Hilger, Bristol, 1983).
[67] D.J. Ben Daniel and C.B. Duke, Phys. Rev. **152**, 683 (1966).
[68] W.W. Rühle, K. Leo, and E. Bauser, Phys. Rev. B **40**, 1756 (1989).
[69] K.J. Moore, P.D. Dawson, and C.T. Foxon, Phys. Rev. B **38**, 3368 (1988).
[70] J. Erland, I. Balslev, and J.M. Hvam, in *Coherent Optical Interactions in Semiconductors* (Ref. 28).

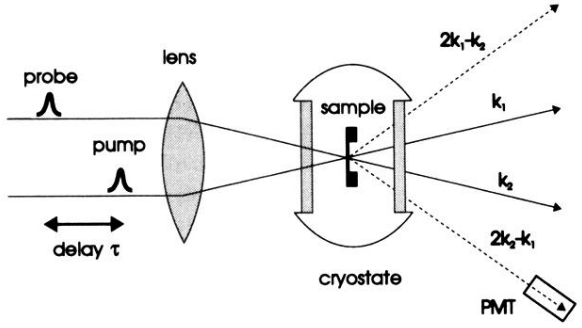

FIG. 3. Scheme of the self-diffracted FWM experiment. The two copolarized beams $\vec{k}_1$ and $\vec{k}_2$ are focused onto the sample, where they create a population grating. Detected is the time-integrated diffracted signal in the background-free direction $\vec{k}_3 = 2\vec{k}_2 - \vec{k}_1$ with a photomultiplier (PMT) as a function of the delay time τ.